ARCHIVIO ISTITUZIONALE
DELLA RICERCA

Alma Mater Studiorum Università di Bologna
Archivio istituzionale della ricerca

distinct: a novel approach to differential distribution analyses

This is the final peer-reviewed author's accepted manuscript (postprint) of the following publication:

*Published Version:*
distinct: a novel approach to differential distribution analyses / Simone Tiberi; Helena L Crowell; Pantelis Samartsidis; Lukas M Weber; Mark D Robinson. - In: THE ANNALS OF APPLIED STATISTICS. - ISSN 1932-6157. - ELETTRONICO. - 17:2 (June)(2023), pp. 1681-1700. [10.1214/22-AOAS1689]

*Availability:*
This version is available at: https://hdl.handle.net/11585/906917 since: 2022-11-28

*Published:*

DOI: http://doi.org/10.1214/22-AOAS1689

*Terms of use:*

Some rights reserved. The terms and conditions for the reuse of this version of the manuscript are specified in the publishing policy. For all terms of use and more information see the publisher's website.

This item was downloaded from IRIS Università di Bologna (https://cris.unibo.it/).
When citing, please refer to the published version.

(Article begins on next page)

02 May 2024

This is the final peer-reviewed accepted manuscript of:

**Simone Tiberi, Helena L. Crowell, Pantelis Samartsidis, Lukas M. Weber, Mark D. Robinson. (2023). "*distinct*: A novel approach to differential distribution analyses". *Annals of Applied Statistics*, Vol. 17, Issue 2, June 2023, pp. 1681-1700.**

The final published version is available online at:
**https://doi.org/10.1214/22-AOAS1689**

Terms of use:

Some rights reserved. The terms and conditions for the reuse of this version of the manuscript are specified in the publishing policy. For all terms of use and more information see the publisher's website.

*This item was downloaded from IRIS Università di Bologna (https://cris.unibo.it/)*

***When citing, please refer to the published version.***

# *distinct*: a novel approach to differential distribution analyses

Simone Tiberi[1*], Helena L Crowell[1], Pantelis Samartsidis[2], Lukas M Weber[3] and Mark D Robinson[1]

[1] *Department of Molecular Life Sciences and Swiss Institute of Bioinformatics, University of Zurich, Zurich, Switzerland.*
[2] *MRC Biostatistics Unit, School of Clinical Medicine, University of Cambridge, Cambridge, UK.*
[3] *Department of Biostatistics, Johns Hopkins Bloomberg School of Public Health, Baltimore, MD, USA.*
[*] e-mail: Simone.Tiberi@uzh.ch

## Abstract

**We present *distinct*, a general method for differential analysis of full distributions that is well suited to applications on single-cell data, such as single-cell RNA sequencing and high-dimensional flow or mass cytometry data. High-throughput single-cell data reveal an unprecedented view of cell identity and allow complex variations between conditions to be discovered; nonetheless, most methods for differential expression target differences in the mean and struggle to identify changes where the mean is only marginally affected. *distinct* is based on a hierarchical non-parametric permutation approach and, by comparing empirical cumulative distribution functions, identifies both differential patterns involving changes in the mean, as well as more subtle variations that do not involve the mean. We performed extensive benchmarks across both simulated and experimental datasets from single-cell RNA sequencing and mass cytometry data, where *distinct* shows favourable performance, identifies more differential patterns than competitors, and displays good control of false positive and false discovery rates. *distinct* is available as a Bioconductor R package.**

**keywords:** Differential distribution; Differential analyses; Differential state; High-throughput single-cell data; Single-cell RNA-seq; Single-cell flow and mass cytometry; Permutation tests.

## Background

Technology developments in the last decade have led to an explosion of high-throughput single-cell data, such as single-cell RNA sequencing (scRNA-seq) and high-dimensional flow or mass cytometry data, allowing researchers to investigate biological mechanisms at single-cell resolution. Single-cell data have also extended the canonical definition of differential expression by displaying cell-type specific responses across conditions, known as differential state (DS) [32], where genes or proteins vary in specific sub-populations of cells (e.g., a cytokine response in myeloid cells but not in other leukocytes [13]). Classical bulk differential expression methods have been shown to perform well when used on single-cell measurements [25, 26, 31] and on aggregated data (i.e., averages or sums across cells), also referred to as pseudo-bulk (PB) [7, 32]. However, most bulk and PB tools focus on shifts in the means, and may conceal information about cell-to-cell heterogeneity. Indeed, single-cell data can show more complex variations (Figure 1 and Supplementary Figure 1); such patterns can arise due to increased stochasticity and heterogeneity, for example owing to oscillatory and unsynchronized gene expression between cells, or when some cells respond differently to a treatment than others [15, 31]. In addition to bulk and PB tools, other methods were specifically proposed to perform differential analyses on single-cell data (notably: *scDD* [15], *SCDE* [14], *MAST* [11], *BASiCS* [10, 29, 30] and mixed models [27]). Nevertheless, they all present significant limitations: BASiCS does not perform cell-type specific differential testing between conditions, scDD does not directly handle covariates and biological replicates, while PB, SCDE, MAST and mixed models performed poorly in previous benchmarks when detecting differential patterns that do not involve the mean [7, 15].

## Results

### *distinct*'s full distribution approach

To overcome these challenges, we developed *distinct*, a flexible and general statistical methodology to perform differential analyses between groups of distributions.

*distinct* is particularly suitable to compare groups of samples (i.e., biological replicates) on single-cell data.

Our approach computes the empirical cumulative distribution function (ECDF) from the individual (e.g., single-cell) measurements of each sample, and compares ECDFs to identify changes between full distributions, even when the mean is unchanged or marginally involved (Figure 1 and Supplementary Figure 1). First, we compute the ECDF of each individual sample; then, we build a fine grid and, at each cut-off, we average the ECDFs within each group, and compute the absolute difference between such averages. A test statistic, $s^{obs}$, is obtained by adding these absolute differences.

More formally, assume we are interested in comparing two groups, that we call $A$ and $B$, for which $N_A$ and $N_B$ samples are available, respectively. The ECDF for the $i$-th sample in the $j$-th group, is denoted by $ecdf_i^{(j)}(.)$, for $j \in \{A, B\}$ and $i = 1, \dots, N_j$. We then define $K$ equally spaced cut-offs between the minimum, $min$, and maximum, $max$, values observed across all samples: $b_1, \dots, b_K$, where $b_k = min + k \times l$, for $k = 1, \dots, K$, with $l = (max - min)/(K + 1)$ being the distance between two consecutive cut-offs. We exclude $min$ and $max$ from the cut-offs because, trivially, $ecdf_i^{(j)}(min) = 0$ and $ecdf_i^{(j)}(max) = 1$, $\forall j, i$. At every cut-off, we compute the absolute difference between the mean ECDF in the two groups; our test statistic, $s^{obs}$, is obtained by adding these differences across all cut-offs:

$$s^{obs} = \sum_{k=1}^{K} \left| \frac{\sum_{i=1}^{N_A} ecdf_i^{(A)}(b_k)}{N_A} - \frac{\sum_{i=1}^{N_B} ecdf_i^{(B)}(b_k)}{N_B} \right|. \quad (1)$$

Note that in differential state analyses, these operations are repeated for every gene-cluster combination.

Intuitively, $s^{obs}$, which ranges in $[0, \infty)$, approximates the area between the average ECDFs, and represents a measure of distance between two groups of densities: the bigger $s^{obs}$, the greater the distance between groups. The number of cut-offs $K$, which can be defined by users, is set to 25 by default, because no detectable difference in performance was observed when further increasing it (data not shown). Note that, although at each cut-off we compute the average across each group's curves, ECDFs are computed separately for each individual sample, therefore our approach still accounts for the within-group variability; indeed, at a given threshold, the average of the sample-specific ECDFs differs from the group-level ECDF (i.e., the curve based on all individual measurements from the group). The null distribution of $s^{obs}$ is then estimated via a hierarchical non-parametric permutation approach (see Methods). A major disadvantage of permutation tests, which often restricts its usage on biological data, is that too few permutations are available from small samples. We overcome this by permuting cells, which is still possible in small samples, because there are many more cells than samples. In principle, this may lead to an inflation of false positives due to lack of exchangability (see Methods); nonetheless, in our analyses, *distinct* provides good control of both false positive and false discovery rates.

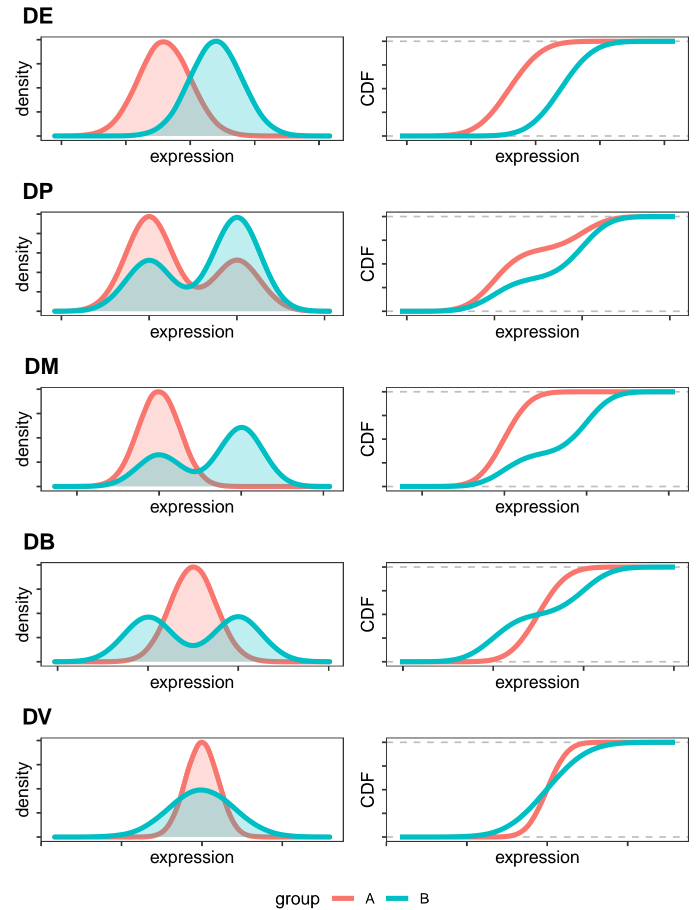


**Figure 1: Cumulative distribution functions (CDFs) unravel differences between distributions.** Density (left panels) and CDF (right panels) of five differential patterns: differential variability (DV), and the four proposed by Korthauer et. al. [15]: differential expression (DE), differential proportion (DP), differential modality (DM), and both differential modality and different component means (DB).

Importantly, *distinct* is general and flexible: it targets complex changes between groups, explicitly models biological replicates within a hierarchical framework, does not rely on asymptotic theory, avoids parametric assumptions, and can be applied to arbitrary types of data. Additionally, *distinct* can also adjust for sample-level cell-cluster specific covariates (i.e., whose effect varies across cell clusters), such as batch effects. In particular, *distinct* fits a linear mixed effects model with

the input data (e.g., normalized counts) as response variable, nuisance covariates as fixed effects, and samples as random effects. The method then removes the estimated impact of fixed effect covariates, and performs differential testing on these normalized values (see Methods).

Furthermore, to enhance the interpretability of differential results, *distinct* provides functionalities to compute (log) fold changes between conditions, and to plot densities and ECDFs, both for individual samples and at the group-level.

Note that, although *distinct* and the Kolmogorov-Smirnov [18] (KS) test share similarities (they both compare distributions via non-parametric tests), the two approaches present several conceptual differences. Firstly, the KS considers the maximum distance between two ECDFs, while our approach estimates the overall distance between ECDFs, which in our view is a more appropriate way to measure the difference between distributions. Secondly, the KS test only compares two individual densities, while our framework compares groups of distributions. Thirdly, while the KS statistic relies on asymptotic theory, our framework uses a permutation test. Finally, a comparison between *distinct* and *scDD* [15] based on the KS test (labelled *scDD-KS*) shows that our method, compared to the KS test, has greater statistical power to detect differential effects and leads to fewer false discoveries (see Simulation studies).

## Simulation studies

We conducted an extensive benchmark, based on scRNA-seq and mass cytometry simulated and experimental datasets to investigate *distinct*'s ability to identify differential patterns in sub-populations of cells.

First, we simulated droplet scRNA-seq data via *muscat* [7] (see Methods). We ran five simulation replicates for each of the differential profiles in Figure 1, with 10% of the genes being differential in each cluster, where DE (differential expression) indicates a shift in the entire distribution, DP (differential proportion) implies two mixture distributions with different proportions of the two components, DM (differential modality) assumes a unimodal and a bimodal distribution, DB (both differential modality and different component means) compares a unimodal and a bimodal distribution with the same overall mean, and DV (differential variability) refers to two unimodal distributions with the same mean but different variance (Figure 1 and Supplementary Figure 1). Each individual simulation consists of 4,000 genes, 3,600 cells, separated into 3 clusters, and two groups of 3 samples each, corresponding to an average of 200 cells per sample in each cluster.

We considered six different normalization approaches: counts per million (CPMs), *scater*'s logcounts [19], *linnorm* [34], *BASiCS* [10,29,30], *SCnorm* [3] and residuals from variance stabilizing normalization from *sctransform* (vstresiduals) [12]. We compared *distinct* to several PB approaches from *muscat*, based on *edgeR* [24], *limma-voom* and *limma-trend* [23], which emerged among the best performing methods for differential analyses from scRNA-seq data [7,26]. We further considered three methods from *muscat* based on mixed models (MM), namely *MM-dream2*, *MM-vstresiduals* and *MM-nbinom* (see Methods). Finally, we included *scDD* [15], which is conceptually similar to our approach: *scDD* implements a non-parametric method to detect changes between individual distributions from scRNA-seq, based on the Kolmogorov-Smirnov test, *scDD-KS*, and on a permutation approach, *scDD-perm*. For *scDD-perm* we used 100 permutations to reduce the computational burden.

In all scenarios and on all six input data, *distinct* shows favourable performance: it has good statistical power while controlling for the false discovery rate (FDR) (Figure 2). In particular, for DE, DP and DM, *distinct* has similar performance to the best performing competitors (*edgeR.linnorm* and *limma-trend.logcounts*), while for DB and DV, it achieves significantly higher true positive rate (TPR), especially when using *logcounts*. PB methods in general perform well for differential patterns involving changes in the mean (DE, DP and DM), but struggle to identify DB and DV patterns. *scDD* provides good TPR across all patterns when using the KS test on vstresiduals (*scDD-KS.vstresiduals*), while the TPR is significantly reduced when using other inputs and with the permutation approach(*scDD-perm*); however, *scDD* methods (in particular, *scDD-KS.vstresiduals*) also show a significant inflation of the FDR. In contrast, MM methods provide good control of the FDR but have low statistical power in all differential scenarios. We also investigated how normalization influences each method's results (Supplementary Figure 2): *distinct* appears to be the least affected method and displays the smallest variation across normalization inputs, possibly due to its non-parametric structure, which can more flexibly accommodate various inputs. Given the computational cost of *SCnorm*, which is significantly higher than the other normalizations, we only included this approach in the results from the main simulations. Furthermore, among the 25 replicate datasets in Figure 2, *SCnorm* ran in a few minutes on 10 simulations, while it failed to run within a week time

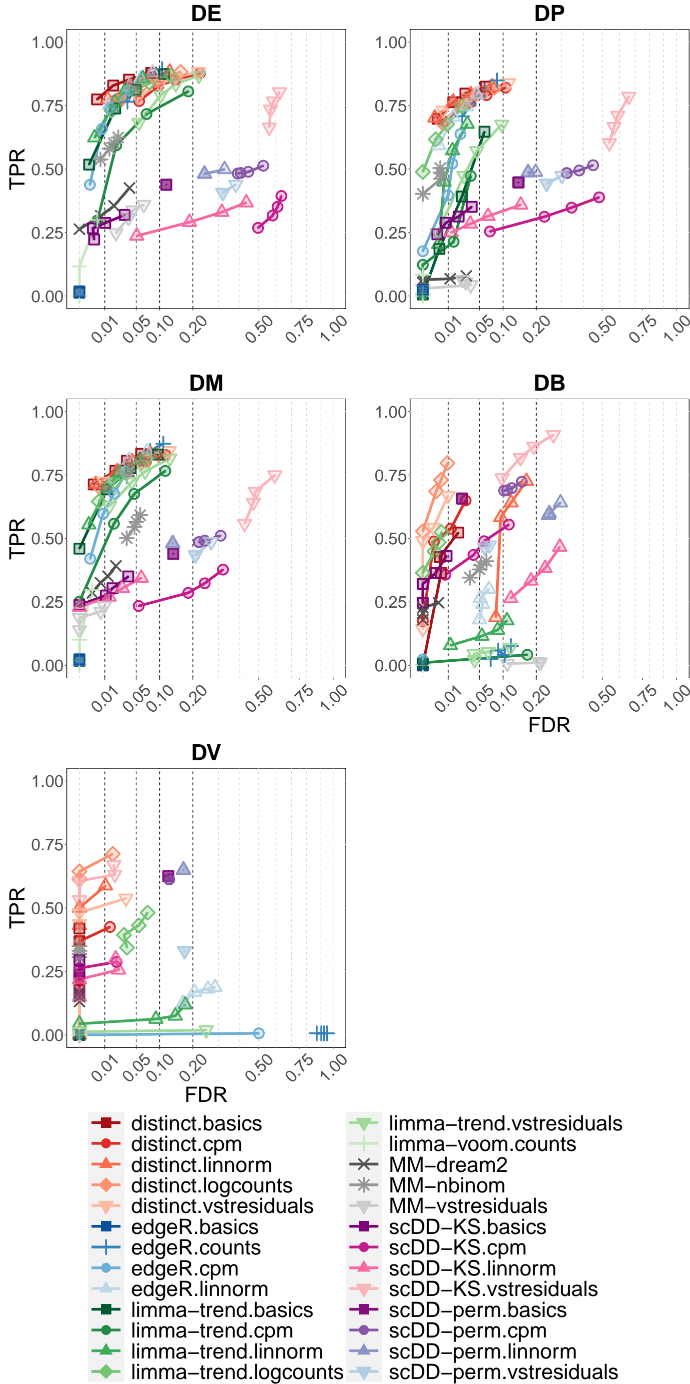


**Figure 2: *distinct* identifies various differential patterns and controls for the FDR.** TPR *vs.* FDR in *muscat* simulated data; DE, DP, DM, DB and DV refer to the differential profiles illustrated in Figure 1. Circles indicate observed FDR for 0.01, 0.05, 0.1 and 0.2 significance thresholds. Results are averages across the five simulation replicates. Each individual replicate consists of 4,000 genes, 3,600 cells, separated into 3 clusters, and two groups of 3 samples each, corresponding to an average of 200 cells per sample in each cluster.

242 (on 10 cores) on the remaining 15 datasets. Therefore,
243 we excluded *SCnorm* from Figure 2 and, in Supple-
244 mentary Figures 3 and 4, we report a comparison of
245 *SCnorm* to the remaining normalization methods, on
246 the subset of 10 simulations where all normalizations
247 successfully ran. For *distinct*, *edgeR* and *limma*, no no-
248 ticeable differences are detected between *SCnorm* and

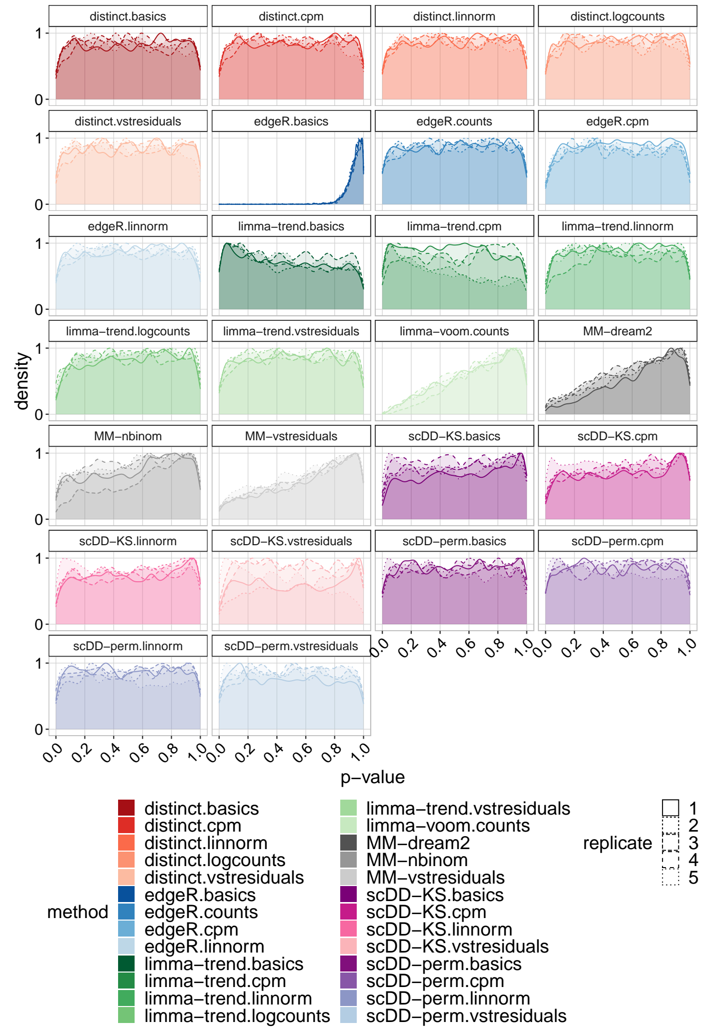


**Figure 3: *distinct* has uniform null p-values.** Density of raw p-values in *muscat* null simulated data; each replicate represents a different null simulation. Each individual replicate consists of 4,000 genes, 3,600 cells, separated into 3 clusters, and two groups of 3 samples each, corresponding to an average of 200 cells per sample in each cluster.

249 the remaining normalization methods, while for *scDD-*
250 *KS SCnorm* leads to a higher inflation of the FDR.

251 We further simulated five null simulation replicates
252 with no differential patterns; again with each simulation
253 having 4,000 genes, 3,600 cells, 3 cell clusters and two
254 groups of 3 samples each. In the null simulated data,
255 only *limma-trend.basics* and *limma-trend.cpm* present a
256 mild inflation of false positives, while MM and, particu-
257 larly, *edgeR.basics* lead to overly conservative p-values;
258 instead, *distinct* and *scDD* show approximately uni-
259 form p-values for all types of input data (Figure 3).

260 We also extended previous simulations to add a cell-
261 type specific batch effect (i.e., a batch effect that affects
262 differently each cell-type) [7,17]. In particular, we sim-
263 ulated 2 batches, that we call $b_1$ and $b_2$, with one group
264 of samples having two samples associated to $b_1$ and one
265 to $b_2$, and the other group of samples having two sam-
266 ples from batch $b_2$ and one from $b_1$. Differential results

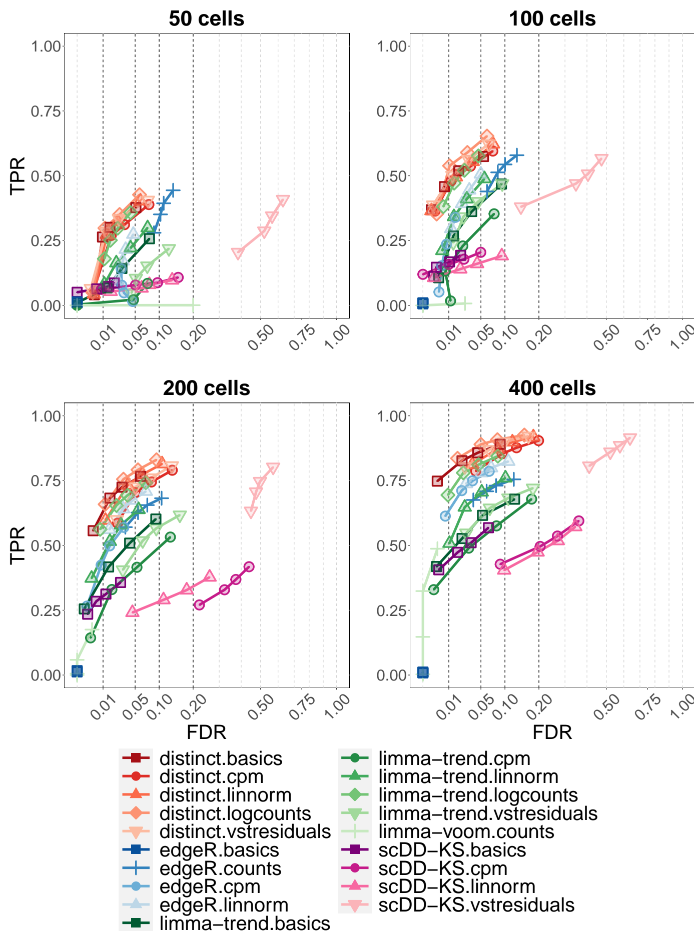


**Figure 4: *distinct* achieves good performance when varying the number of available cells.** TPR *vs.* FDR in *muscat* simulated data; with 50, 100, 200 and 400 cells per cluster-sample combination, corresponding to a total of 900, 1,800, 3,600 and 7,200 cells, respectively. Results are aggregated over the five replicate simulations of each differential type (DE, DP, DM, DB and DV), contributing in equal fraction. Each individual simulation replicate consists of 4,000 genes, 3 cell clusters and two groups of 3 samples each. Circles indicate observed FDR for 0.01, 0.05, 0.1 and 0.2 significance thresholds. Note that *scDD-perm* and MM were excluded from this analysis due to their computational cost.

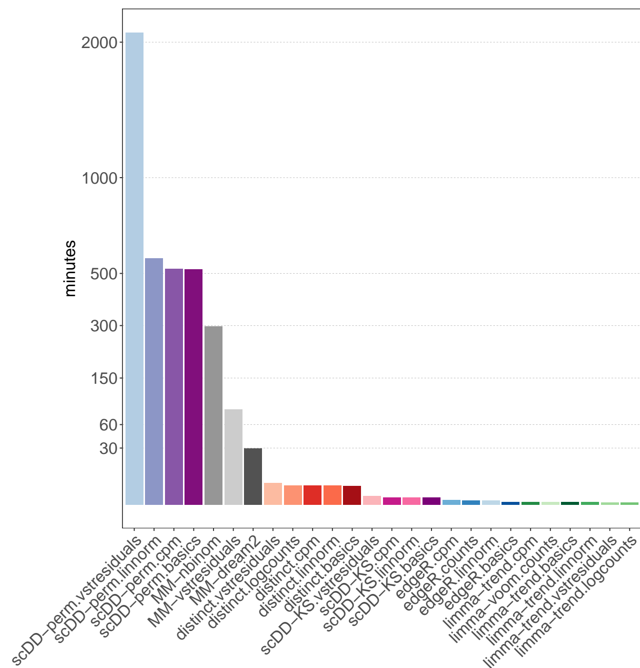


**Figure 5: *distinct* requires more computational resources than PB and *scDD-KS* methods, but significantly less than MM and *scDD-perm* models.** Average computing time, expressed in minutes, in *muscat* main simulations (Figures 2-3). For each method, times are averaged across simulation types (DE, DP, DM, DB, DV and null) and, for each type, across the five replicate simulations; in each replicate 3,600 cells are available (200, on average, per cluster-sample combination). *distinct*, MM and *scDD* models were run on 3 cores, while pseudo-bulk methods based on *edgeR* and *limma* used a single core because they do not allow for parellel computing. Note that *scDD-perm* requires much longer on vstresiduals than on the other normalized data, because *scDD* performs differential testing on non-zero values: vstresiduals, (unlike linnorm, cpm and basics normalized data) are not zero-inflated and, therefore, many more cells have to be used for differential testing.

267 are substantially unchanged (Supplementary Figure 5), 268 which shows *distinct* can effectively remove nuisance 269 confounders.

270 Furthermore, we performed various sensitivity analyses 271 and investigated how results are affected when varying: 272 i) the number of cells, ii) the library size, iii) the dis-273 persion parameter, iv) the fraction of significant genes, 274 and v) the sample sizes in each group. In particular, we 275 simulated 50, 100, 200 (as in the original simulation) 276 and 400 cells per sample in each cluster. We further 277 modified the library size and dispersion parameters of 278 the negative binomial model used by *muscat* to simu-279 late scRNA-seq data, influencing the mean expression 280 and cell-to-cell variability respectively, by considering 281 values 1/5, 1/2, 2 and 5 times as big as those used in 282 the original simulation. In addition, we varied the per-283 centage of simulated differential genes as 1, 5, 10 (as in 284 the original simulation) and 20%, and considered var-285 ious unbalanced designs by comparing two groups of 286 different sample sizes: 3 *vs.* 2, 4 *vs.* 3, and 5 *vs.* 3. 287 Overall, increasing the number of cells or the library 288 size and decreasing the dispersion have a positive im-289 pact on the performance of all methods, by improving 290 their ability to detect differential effects (i.e., true pos-291 itive rate); nonetheless, none of these factors seem to 292 affect the relative ranking of methods, which remains 293 globally stable (Figure 4 and Supplementary Figures 294 6-7). In addition, changing the fraction of significant 295 genes and considering unbalanced designs does not ap-296 pear to introduce systematic changes in performance 297 (Supplementary Figures 8-9). Note that, in these sen-298 sitivity analyses, we excluded MM models due to the 299 high computational cost and low statistical power dis-300 played in the previous analyses.

301 From a computational perspective, *distinct* required 302 an average time of 3.2 to 4.5 minutes per simulation, 303 which is higher than PB methods (0.1 to 0.2 minutes)

and *scDD-KS* (0.5 to 0.7 minutes), but significantly lower than MM approaches (29.4 to 297.3 minutes) and *scDD-perm* (544.7 to 2085.6 minutes) (Figure 5 and Supplementary Table 1). All methods were run on 3 cores, except PB approaches, which used a single core, because they do not allow for parellel computing.

We also considered an alternative popular droplet scRNA-seq data simulator, *SplatPOP* [2], which represents a generalization of *Splatter* [35], that allows multi-sample multi-group synthetic data to be generated. In particular, we simulated 20,345 genes from a human genome with two groups of 4 samples each, and 100 cells per sample, belonging to the same cluster of cells, for a total of 800 cells across all samples. We ran 8 differential simulations, with 10% of genes truly differential between groups, by varying the location (*de.facLoc*) and scale (*de.facScale*) differential parameters, mainly affecting the mean and variance, respectively (see Methods). We considered the same normalization and differential methods as in the *muscat* simulation (except MM and *scDD-perm*, which were not considered due to the high computational cost and low statistical power displayed above). As expected, for all methods, differential patterns are easier to detect as the magnitude of the difference increases, with differential location patterns having a higher true positive rate than differential scale patterns. While all methods control the FDR, in all simulations, *distinct* achieves substantially higher TPR than competitors (Figure 6). We also repeated the same simulations including a batch effect, with two batches, with the same scale and location differential parameters for the batch and group differences (i.e., increasing together from 0.2 to 1.5). Again, we excluded *scDD* from these analyses because it cannot handle covariates directly. Results agree with those from the *muscat* batch effect simulation study: FDR and TPRs are mostly unchanged when introducing nuisance covariates, with only a minor decrease in the TPR in stronger batch effects, i.e., when de.facLoc and de.facScale are 1 and 1.5 (Supplementary Figure 10), which again indicates that *distinct* can effectively control for nuisance covariates.

We further considered the semi-simulated mass cytometry data from Weber *et al.* [32] (labelled *diffcyt* simulation), where spike-in signals were computationally introduced in experimental data [5], hence maintaining the properties of real biological data while also embedding a known ground truth signal. We evaluated *distinct* and two methods from *diffcyt*, based on *limma* [23] and linear mixed models (LMM), which outperformed competitors on these same data [32]. In particular, we considered three datasets from Weber

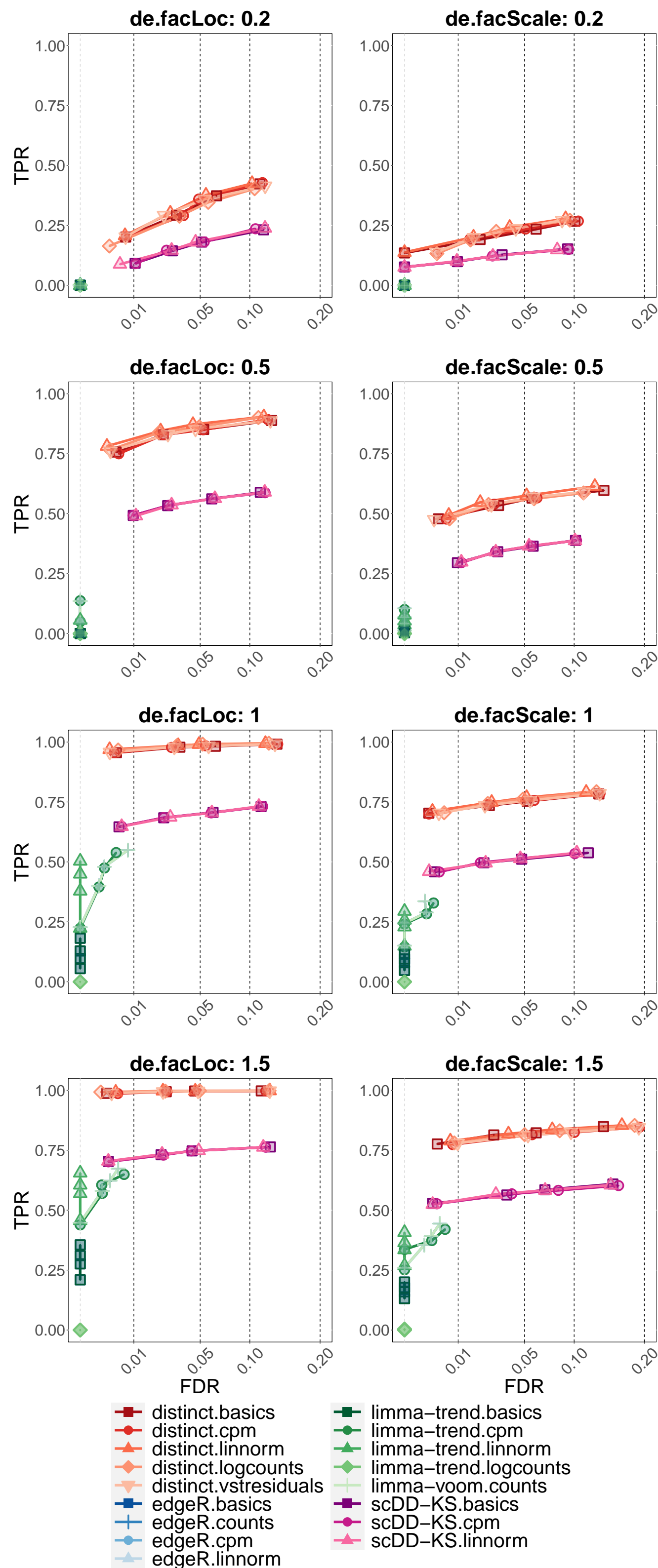


**Figure 6: *distinct* displays higher TPR than competitors.** TPR *vs.* FDR in *SplatPop* simulated data, with various degrees of differential location (left) and scale (right) parameters, primarily affecting the mean and variance, respectively. Circles indicate observed FDR for 0.01, 0.05, 0.1 and 0.2 significance thresholds. Each simulation consists of 20,345 genes genes, 800 cells (belonging to the same cluster), and two groups of 4 samples each, corresponding to an average of 100 cells per sample.

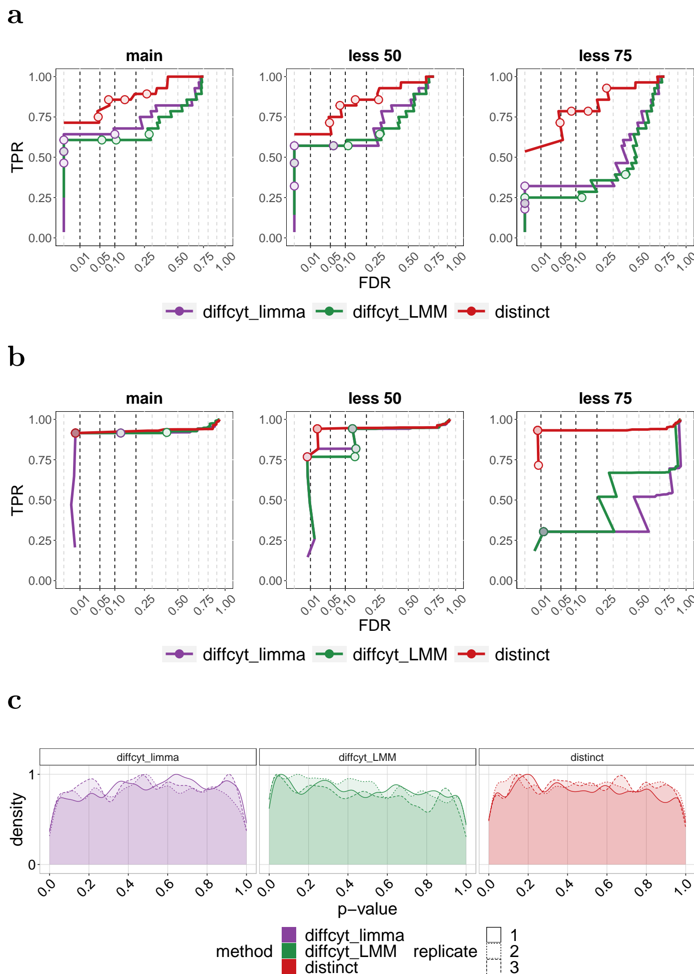


**Figure 7: *distinct* shows high power while controlling for false positive and false discovery rates. (a-b)** TPR *vs.* FDR in *diffcyt* semi-simulated data. 'main', 'less 50' and 'less 75' indicate the main simulation, and those where differential effects are diluted by 50 and 75%, respectively. Each simulation consists of 88,435 cells and two groups of 8 samples each. Circles indicate observed FDR for 0.01, 0.05, 0.1 and 0.2 significance thresholds. **(a)** As in the *muscat* simulation study, cells were clustered into 8 populations based on manually annotated cell types [32]. **(b)** As in Weber *et al.* [32], cells were grouped in 100 high-resolution clusters via unsupervised clustering. **(c)** Density of raw p-values in *diffcyt* null semi-simulated data; each replicate represents a different null simulation. Each replicate consists of 88,438 cells and two groups of 8 samples each. As in Weber *et al.* [32], cells were clustered in an unsupervised manner.

*et al.* [32]: the main DS dataset and two more where differential effects were diluted by 50 and 75%. Each dataset consists of 24 protein markers, 88,435 cells, and two groups (with and without spike-in signal) of 8 samples each. Measurements were first transformed, and then cells were grouped into sub-populations with two separate approaches (see Methods): i) similarly to the *muscat* simulation study, cell labels were defined based on 8 manually annotated cell types [32] (Figure 7a), and ii) as in the original *diffcyt* study from Weber *et al.* [32], cells were grouped into 100 high-resolution clusters (based on 10 cell-type markers, see Methods) via unsupervised clustering (Figure 7b). In the main simulation, *distinct* achieves higher TPR when considering cell-type labels (Figure 7a, 'main'), while all methods exhibit substantially overlapping performance when using unsupervised clustering (Figure 7b, 'main'). In both clustering approaches, as the magnitude of the differential effect decreases, the distance between methods increases: *diffcyt* tools show a significant drop in the true positive rate whereas *distinct* maintains a higher TPR while effectively controlling for the false discovery rate (FDR) (Figures 7a-b and Supplementary Figure 11). This indicates that *distinct* has good statistical power to detect even small changes between conditions. We also considered the three replicate null datasets from Weber *et al.* [32] (i.e., with no differential effect), containing 24 protein markers and 88,438 cells across 8 cell types, and found that all methods display approximately uniform p-values (Figure 7c).

## Experimental data analyses

In order to investigate false positive rates (FPRs) in real data, we considered two experimental scRNA-seq datasets where no differential signals were expected, by comparing samples from the same experimental condition. Given the high computational cost and low power of MM, and the high FDR of *scDD* models, for the real data analyses, we only included *distinct* and PB methods. We considered gene-cluster combinations with at least 20 non-zero cells across all samples. The first dataset (labelled *T-cells*) consists of a Smart-seq2 scRNA-seq dataset of 19,875 genes and 11,138 T cells isolated from peripheral blood from 12 colorectal cancer patients [36]. We automatically separated cells in 11 clusters (via *igraph* [1, 8]), and generated replicate datasets, by randomly separating, three times, the 12 patients to two groups of size 6. The second dataset (labelled *Kang*) contains 10x droplet-based scRNA-seq peripheral blood mononuclear cell data from 8 Lupus patients, before (controls) and after (stimulated) 6h-treatment with interferon-$\beta$ (INF-$\beta$), a cytokine known to alter the transcriptional profile of immune cells [13]. The full dataset contains 35,635 genes and 29,065 cells, which are separated (via manual annotation [13]) into 8 cell types. One of the 8 patients was removed as it appears to be a potential outlier (Supplementary Figures 12-14). Here we only included singlet cells and cells assigned to a cell population, and considered control samples only, resulting in 11,854 cells and 10,891 genes. Again, we artificially created three replicate datasets by randomly assigning the 7 retained control samples in two groups of size 3 and 4. In both null analyses, we found that *limma-trend*, particularly when using CPMs, leads to an increase of FPRs, *distinct*'s p-values are only

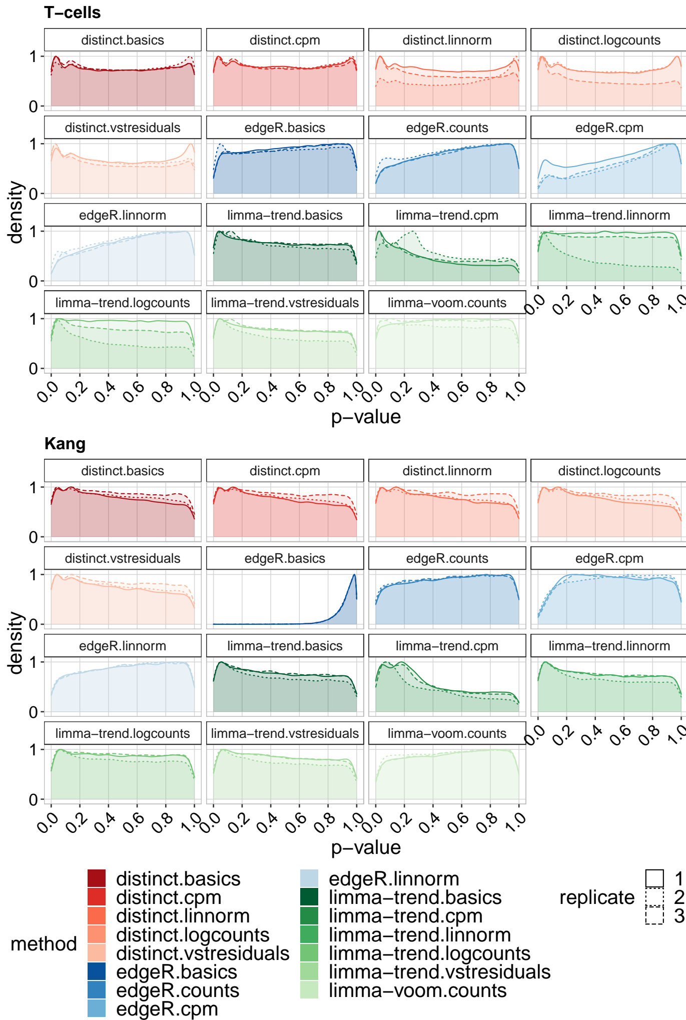


**Figure 8: On experimental scRNA-seq data, *distinct* has almost-uniform null p-values.** Density of raw p-values in the null *T-cells* (top) and *Kang* (bottom) experimental data. Each replicate represents a random partition of samples in two groups. The *T-cells* data consists of 12 samples and 11,138 cells across 11 clusters. For the *Kang* dataset, we retained 7 samples and 11,854 cells across 8 clusters.

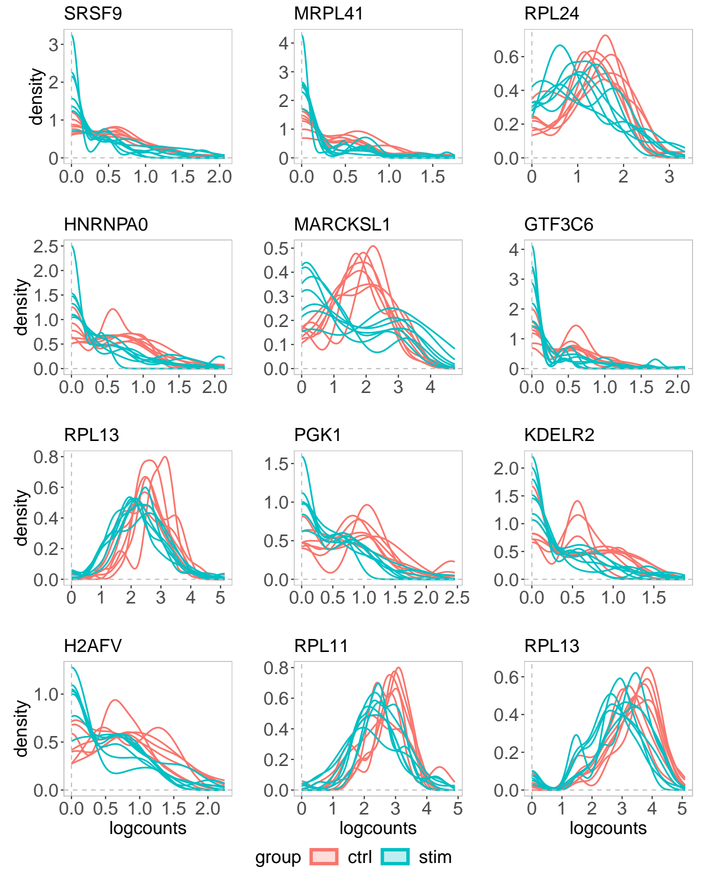


**Figure 9: *distinct* discovers non-canonical differential patterns.** Density of logcounts for nine examples of differential patterns identified by *distinct* on all input data (adjusted p-values $< 0.05$), and not by any PB tool (adjusted p-values $> 0.05$), on the *Kang* dataset when comparing controls and stimulated samples. Gene RPL13 was identified in FCGR3A+ Monocytes (third row) and in NK cells (fourth row), while all other genes were detected in Dendritic cells. Each line represents a sample.

420 marginally inflated towards 0, while *edgeR* and *limma-*
421 *voom* are the most conservative methods and provide
422 the best control of FPRs (Figure 8 and Supplemen-
423 tary Tables 2-3). Regarding normalization, *linnorm*
424 and *BASiCS* lead to the most conservative p-values and
425 smallest false positive rates.

426 We then considered again the *Kang* dataset, and per-
427 formed a DS analysis between controls and stimulated
428 samples. Again, we removed one potential outlier pa-
429 tient, and only considered singlet cells and cells as-
430 signed to a cell population; we further filtered gene-
431 cluster combinations with less than 20 non-zero cells
432 across all samples, resulting in 12,045 genes and 23,571
433 cells across 8 cell types and 14 samples. We found
434 that *distinct* identifies more differential patterns than
435 PB methods, with *edgeR* and *limma-voom* being the
436 most conservative methods, and that its results are
437 very coherent across different input data (Supplemen-
438 tary Figure 15). When visually investigating the gene-
439 cluster combinations detected by *distinct* (adjusted p-
440 value $< 0.1$), on all five input data (CPMs, logcounts,
441 linnorm, BASiCS and vstresiduals), and not detected
442 by any of the ten PB approaches (adjusted p-value $>$
443 $0.1$), we found several interesting non-canonical differ-
444 ential patterns (Figure 9 and Supplementary Figures
445 16-27). In particular, gene MARCKSL1 displays a DB
446 pattern, with stimulated samples having higher density
447 on the tails and lower in the centre of the distribu-
448 tion, gene RPL13 mirrors classical DE, while the other
449 genes seem to emulate DP profiles. Interestingly, ten
450 out of eleven of these genes are known tumor prog-
451 nostic markers: H2AZ2 for cervical and renal cancer,
452 SRSF9 for liver cancer and melanoma, RPL24 for re-
453 nal and thyroid cancer, HNRNPA0 for renal and pan-
454 creatic cancer, MARCKSL1 for liver and renal cancer,
455 GTF3C6 for liver cancer, RPL13 for endometrial and
456 renal cancer, PGK1 for breast, head and neck, cervical,
457 liver, and pancreatic cancer, KDELR2 for renal, head

| method | % of unique results |
|---|---|
| distinct.logcounts | 0.3 |
| distinct.basics | 0.8 |
| limma-trend.logcounts | 0.9 |
| distinct.cpm | 1.0 |
| distinct.vstresiduals | 1.1 |
| edgeR.linnorm | 1.2 |
| limma-trend.vstresiduals | 1.5 |
| limma-trend.basics | 1.5 |
| edgeR.counts | 1.7 |
| edgeR.basics | 3.0 |
| distinct.linnorm | 3.6 |
| limma-trend.linnorm | 3.7 |
| limma-voom.counts | 5.6 |
| edgeR.cpm | 10.4 |
| limma-trend.cpm | 26.8 |

**Table 1:** Percentage of unique gene/cell-type identifications that are unique to each method. Since methods return significantly different number of significant results, for each method, we selected the most significant 1,000 results. For every method, we then compute the fraction of such results that are unique, i.e., not in common with the top 1,000 results returned by any other method.

458 and neck and glioma cancer, and RPL11 for renal and 459 breast cancer [28]. This is an interesting association, 460 considering that INF-$\beta$ stimulation is known to inhibit 461 and interfere with tumor progression [9, 22]. Addition-462 ally, Supplementary Figures 16-27 show how *distinct* 463 can identify differences between groups of distributions 464 even when only a portion of the ECDF varies between 465 conditions. Finally, we computed the fraction of de-466 tected genes that are unique by each method. Given 467 that a ground truth is absent, we speculate that gene-468 cluster combinations detected by multiple methods are 469 more likely to be truly differential, while those detected 470 by a single method are more likely to be false posi-471 tive detections. Since methods return widely different 472 number of significant genes, for each method, we con-473 sidered the top (i.e., smallest p-value) 1,000 genes per 474 cell-type. We then computed the percentage of results 475 that are unique to each method (Table 1), i.e., not in 476 common with the top 1,000 results returned by any 477 other method. Overall, *distinct* displays a lower frac-478 tion of unique results (1.4% on average across all input 479 data) compared to *edgeR* (4%) and *limma* (6.7%). It is 480 also interesting to note that *scater*'s logcounts normal-481 ization lead to the 2 smallest fractions of unique values 482 (i.e., *distinct.logcounts* and *limma-trend.logcounts*).

# 483 Discussion

484 High-throughput single-cell data can display complex 485 differential patterns; nonetheless, most methods for dif-486 ferential expression fail to identify changes where the 487 mean is not affected. To overcome the limitations of 488 present differential tools, we have developed *distinct*, a 489 novel method to identify differential patterns between 490 groups of distributions, which is particularly well suited 491 to perform differential analyses on high-throughput 492 single-cell data. *distinct* is based on a flexible hier-493 archical multi-sample full-distribution non-parametric 494 approach. In order to compare it to state-of-the-art 495 differential methods, we ran extensive benchmarks on 496 both simulated and experimental datasets from scRNA-497 seq and mass cytometry data, where our approach ex-498 hibits favourable performance, provides good control of 499 the FNR and FDR, and is able to identify more patterns 500 of differential expression compared to canonical tools, 501 even when the overall mean is unchanged. In particular, 502 our approach displays a higher statistical power (i.e., 503 TPR) not only than PB methods, but also compared 504 to other non-parametric frameworks from *scDD*, based 505 on the Kolmogorov-Smirnov test statistic (*scDD-KS*) 506 and on permutation tests (*scDD-perm*). *distinct* also 507 allows for biological replicates, does not rely on asymp-508 totic theory, which could be inaccurate in small sample 509 sizes (typical of biological data), and avoids parametric 510 assumptions, that may be challenging to meet in single-511 cell data. Additionally, *distinct* can also effectively ad-512 just for sample-level cell-cluster specific covariates (i.e., 513 whose effect varies across cell clusters), such as batch 514 effects (Supplementary Figure 5). Importantly, *distinct* 515 is a very general test that, due to its non-parametric 516 nature, can be applied to various types of data, even 517 beyond the single-cell applications shown here. Fur-518 thermore, thanks to its flexible form, we have shown in 519 our simulations that *distinct* has the most consistent 520 performance across normalization approaches (Supple-521 mentary Figure 2 and 4).

522 However, these advantages come at the expense of a 523 higher computational burden, particularly when com-524 pared to PB methods or KS approaches (Figure 5). 525 Nonetheless, by employing clever computational tech-526 niques (i.e., parallel computing and C++ coding within 527 R), the method runs within minutes on a laptop, even 528 for large datasets. Overall, we believe that *distinct* 529 represents a valid alternative for differential detections 530 from single-cell data, particularly when interest lies be-531 yond canonical differences in means, as it allows to en-532 hance statistical power at the cost of a reasonable in-533 crease in the computational time.

534 Finally, although we have focused here on comparing 535 two groups of samples, several future extensions are 536 possible to allow our framework to be applied to dif-537 ferent scenarios. For instance, by suitably modifying

the test statistics in (1), one may ideally extend our approach to perform a joint differential test between three of more groups of samples. Although, it is worth noting that, in the presence of three or more experimental conditions, at present, it is still possible to run pairwise comparisons between pairs of conditions. While a joint test across all groups may certainly be of interest in some cases, from our experience, comparisons between pairs of groups are usually more used among scientists. In addition, as we were suggested by a user, *distinct* could be employed to compare cell clusters instead of experimental conditions, hence discovering differential genes between cell clusters (e.g., cell types), even from individual samples.

## Availability

*distinct* is freely available as a Bioconductor R package at: https://bioconductor.org/packages/distinct. The scripts used to run all analyses are available on GitHub (https://github.com/SimoneTiberi/distinct_manuscript, version v3) and Zenodo (DOI: 10.5281/zenodo.6397114). The *diffcyt* simulated data is available via FlowRepository (accession ID FR-FCM-ZYL8 [32]) and *HDCytoData* R Bioconductor package [33]; the *Kang* dataset can be accessed via *muscData* R Bioconductor package [6]; the *T-cells* dataset is deposited on the European Genome-phenome (accession id EGAD00001003910 [36]).

## Acknowledgements

We acknowledge Almut Luetge, Brian D M Tom, Christina Azodi, Davis McCarthy, Reinhard Furrer, and the entire Robinson lab for precious comments and suggestions. This work was supported by Forschungskredit to ST (grant number FK-19-113) as well as by the Swiss National Science Foundation to MDR (grants 310030_175841, CRSII5_177208). MDR acknowledges support from the University Research Priority Program Evolution in Action at the University of Zurich.

## Author contributions

ST conceived the method, implemented it, performed all analyses and wrote the manuscript. ST and MDR designed the study. HLC and LMW contributed to *muscat* and *diffcyt* simulation studies, respectively. PS contributed to the computational development of *distinct* and to the revision process. All authors read, contributed to, and approved the final article.

## Competing interests

The authors declare no competing interests.

# Methods

## Permutation test

In order to test for differences between groups, we employ a hierarchical permutation approach: to estimate the null distribution of $s^{obs}$, we permute the individual observations (e.g., single-cell measurements) instead of the samples. Note that this violates the exchangeability assumption of permutation tests and, hence, p-values are not guaranteed to be uniformly distributed under the null hypothesis; nonetheless, in our simulated and experimental analyses, we empirically show that *distinct* provides good control of both false positive and false discovery rates. We randomly permute individual observations $P$ times across all samples and groups, by retaining the original sample sizes. We denote by $s_p$ the test statistic computed at the $p$-th permutation, $p = 1, \dots, P$. A p-value, $\tilde{p}$, is obtained as [21]:

$$\tilde{p} = \frac{\sum_{p=1}^{P} \mathbf{1}\left(s_p \geq s^{obs}\right) + 1}{P + 1}, \quad (2)$$

where $\mathbf{1}(cond)$ is 1 if $cond$ is true, and 0 otherwise. In order to accurately infer small p-values, when $\tilde{p}$ is below some pre-defined thresholds, the number of permutations are automatically increased and $\tilde{p}$ is re-computed. By default, *distinct* initially computes 100 permutations; when $\tilde{p} \leq 0.1$ these are increased to 500; when the new $\tilde{p} \leq 0.01$ we use $2,000$ permutations, which are further increased to $10,000$ if $\tilde{p} \leq 0.001$. Note that the number of permutations (i.e., 100, 500, 2,000 and 10,000) can be specified by the user.

## Covariates

Assume we observe $Z$ nuisance covariates, and that $N$ samples are available across all groups, where for the $i$-th sample we observe $C_i$ values (e.g., single-cell measurements). We fit the following linear mixed effects model:

$$y_c^{(i)} = \beta_0 + \sum_{z=1}^{Z} \beta_z X_z^{(i)} + \alpha_i + \epsilon_c^{(i)}, \text{ for } i = 1, \dots, N, \text{ and } c = 1, \dots, C_i, \quad (3)$$

where $y_c^{(i)}$ represents the $c$-th observation for the $i$-th sample, $\beta_0$ is the intercept of the model, $X_z^{(i)}$ indicates the $z$-th covariate in the $i$-th sample, $\beta_z$ denotes the

fixed effect coefficient for the $z$-th covariate, $\alpha_i$ represents the random effect term for the $i$-th sample, and $\epsilon_c^{(i)}$ is the (zero-mean) residual for the $c$-th observation in the $i$-th sample. We assume that random terms are normally distributed as $\alpha_i \sim \mathcal{N}(0, \sigma_i^2)$, where $\mathcal{N}(a, b)$ denotes the normal distribution with mean $a$ and variance $b$. Note that, due to the random effect terms, observations from the same sample are positively correlated while, observations between different samples are independent. We infer model parameters via maximum likelihood, with the estimated values for the fixed effect terms denoted by $\hat{\beta}_0, \dots, \hat{\beta}_Z$. We then remove the estimated effect of nuisance covariates as $y_c^{(i)} - \sum_{z=1}^{Z} \hat{\beta}_z X_z^{(i)}$; differential testing is performed, as described above, on these normalized values. In DS analyses, model (3) is fit, separately, for every gene-cluster combination, hence accommodating for cell-type specific effects of covariates.

## Normalization

In scRNA-seq datasets, CPMs and logcounts were computed via *scater* Bioconductor R package [19], vstresiduals were calculated via *sctransform* R package [12] (except for the *T-cells* data, where, due to a failure of *sctransform*'s variance stabilizing normalization, we used *DESeq2*'s vst transformation [16]), while *linnorm*, *BASiCS* and *SCnorm*, normalized data were calculated with the respective Bioconductor R packages [3, 10, 29, 30, 34]. For *SCnorm*, following the author's suggestions, we normalized each cell cluster (3 in total) separately, using samples as *Conditions* parameter.

In mass cytometry datasets, measurements were transformed via *diffcyt*'s *transformData* function, which applies an *arcsinh* transformation.

## *muscat* simulation and *Kang* data

In all *muscat* simulations, we used the control samples of the *Kang* dataset as a anchor data; as in the real data analyses, we excluded one sample as it emerged as a potential outlier (Supplementary Figures 12-14), and only considered singlet cells and cells assigned to a cell population. In *muscat*'s simulation studies, we considered gene-cluster combinations with simulated expression mean greater than 0.2; for DB patterns, we increased this threshold to 1 because with low expression values differences are not visible by eye. In the simulation when varying the library size (Supplementary Figure 6), we filtered gene-clusters combinations with at least 50 non-zero cells. For every simulations, five replicates were simulated, and results were averaged across replicates. In the main simulation (Figure 2) and the batch effect simulation (Supplementary Figure 5), we simulated from a paired design 2 groups of 3 samples each, with 4,000 genes, and 3,600 cells distributed in 3 clusters (corresponding to an average of 200 cells per sample in each cluster). For the simulation study when varying the number of cells (Figure 4), the total numbers of available cells were 900, 1,800, 3,600 and 7,200, corresponding to an average of 50, 100, 200 and 400 cells per sample in every cluster. For the differential simulations, we used log2-FC values of 1 for DE, 1.5 for DP and DM, and 3 for DB and DV. For the batch effect simulation study we used a modified version of *muscat*, developed by Almut Luetge at the Robinson lab (available at: https://github.com/SimoneTiberi/distinct_manuscript), which allows simulating cluster-specific batch effects [7, 17]. All *muscat* simulation studies, as well as the *Kang* non-null data analysis, were performed by editing the original snakemake workflow from Crowell *et al.* [7]. PB methods were applied on aggregated data by summing cell-level measurements; for differential testing, we used *muscat*'s *pbDS* function [7]. Mixed model methods were implemented, via *muscat*'s *mmDS* function, using the same approaches as in Crowell *et al.* [7]: in *MM-dream2* and *MM-vstresiduals* linear mixed models were applied to log-normalized data with observational weights and variance-stabilized data, respectively, while in *MM-nbinom* generalized linear mixed models were fitted directly to raw counts. In the *muscat* simulations and in the *Kang* non-null data analysis, we accounted for the paired design by modelling the patient id as a covariate in all methods that allow for covariates (i.e., *distinct*, PB and MM).

## *splatPop* simulation

In *SplatPOP* simulated data, we used a human genome, version 19, downloaded from https://www.gencodegenes.org/human/release_19.html. We ran a total of 16 simulations: 8 with and 8 without batch effects as nuisance covariate. In each case, we ran 4 differential location ("de.facLoc" parameter) and 4 differential scale ("de.facScale" parameter) simulations, with differential parameters equals to 0.2, 0.5, 1 and 1.5. In every simulation, 10% of genes were differential between groups, and a total of 20,345 genes and 800 cells were simulated (100 per sample). In the simulation with batch effects, the 8 samples were randomly assigned to 2 batches, and the differential location and scale parameters between batches ("batch.facLoc" and "batch.facScale", respectively) matched those between groups of samples

("de.facLoc" and "de.facScale"). For more details on how *SplatPOP*'s data is simulated, please refer to the original manuscript [2] and vignettes.

## *diffcyt* simulation

The *diffcyt* semi-simulated data originates from a real mass cytometry dataset of healthy peripheral blood mononuclear cells from two paired groups of 8 samples each [5]; one group contains unstimulated cells, while the other was stimulated with B cell receptor/Fc receptor cross-linker. The original dataset contains a total of 172,791 cells and 24 protein markers: 10 of these are cell-type markers used for cell clustering, while 14 are cell state markers used for differential state analyses; the distinction between cell state and cell-type markers is based on prior biological knowledge [32]. In Weber *et al.* [32], semi-simulated data were generated by separating the cells of each unstimulated sample in two artificial samples; a differential signal was then computationally introduced by replacing, in one group, unstimulated B cells with B cells from stimulated samples. Measurements were transformed and cells clustered via *diffcyt*'s *transformData* (which applies an *arcsinh* transformation) and *generateClusters* functions, respectively. For the DS simulation in Figure 7b, as in Weber *et al.* [32], we evaluated methods' performance in terms of detecting DS for phosphorylated ribosomal protein S6 (pS6) in B cells, which is the strongest differential signal across the cell types in this dataset [20, 32]. For the DS simulation in Figure 7a, we considered previously manually annotated cell types [32] and included all 14 cell state markers. *diffcyt*'s *limma* and LMM methods were applied via *diffcyt*'s *testDS_limma* and *testDS_LMM* functions, respectively [32]. We accounted for the paired design by modelling the patient id as a covariate.

## P-values adjustment

All p-values were adjusted via Benjamini-Hochberg correction [4]. In *diffcyt* simulations we used globally adjusted p-values for all methods, i.e., p-values from all clusters are jointly adjusted once. However, since PB methods were found to be over-conservative when globally adjusting p-values [7], in *muscat* simulations and *Kang* discovery analyses, we used locally adjusted p-values for all methods.

## Software versions

All analyses were performed via R software version 4.0.0, with Bioconductor packages from release 3.11.

# References


[1] R. A. Amezquita, A. T. Lun, E. Becht, V. J. Carey, L. N. Carpp, L. Geistlinger, F. Marini, K. Rue-Albrecht, D. Risso, C. Soneson, et al. Orchestrating single-cell analysis with bioconductor. *Nature methods*, 17(2):137–145, 2020.

[2] C. B. Azodi, L. Zappia, A. Oshlack, and D. J. McCarthy. splatPop: simulating population scale single-cell RNA sequencing data. *Genome biology*, 22(1):1–16, 2021.

[3] R. Bacher, L.-F. Chu, N. Leng, A. P. Gasch, J. A. Thomson, R. M. Stewart, M. Newton, and C. Kendziorski. Scnorm: robust normalization of single-cell rna-seq data. *Nature methods*, 14(6):584–586, 2017.

[4] Y. Benjamini and Y. Hochberg. Controlling the false discovery rate: a practical and powerful approach to multiple testing. *Journal of the Royal statistical society: series B (Methodological)*, 57(1):289–300, 1995.

[5] B. Bodenmiller, E. R. Zunder, R. Finck, T. J. Chen, E. S. Savig, R. V. Bruggner, E. F. Simonds, S. C. Bendall, K. Sachs, P. O. Krutzik, et al. Multiplexed mass cytometry profiling of cellular states perturbed by small-molecule regulators. *Nature biotechnology*, 30(9):858–867, 2012.

[6] H. L. Crowell. *muscData: Multi-sample multi-group scRNA-seq data*, 2020. R package version 1.1.2.

[7] H. L. Crowell, C. Soneson, P.-L. Germain, D. Calini, L. Collin, C. Raposo, D. Malhotra, and M. D. Robinson. muscat detects subpopulation-specific state transitions from multi-sample multi-condition single-cell transcriptomics data. *Nature Communications*, 11(1):1–12, 2020.

[8] G. Csardi and T. Nepusz. The igraph software package for complex network research. *InterJournal*, Complex Systems:1695, 2006.

[9] M. R. Doherty, H. Cheon, D. J. Junk, S. Vinayak, V. Varadan, M. L. Telli, J. M. Ford, G. R. Stark, and M. W. Jackson. Interferon-beta represses cancer stem cell properties in triple-negative breast cancer. *Proceedings of the National Academy of Sciences*, 114(52):13792–13797, 2017.

[10] N. Eling, A. C. Richard, S. Richardson, J. C. Marioni, and C. A. Vallejos. Correcting the mean-variance dependency for differential variability testing using single-cell RNA sequencing data. *Cell systems*, 7(3):284–294, 2018.

[11] G. Finak, A. McDavid, M. Yajima, J. Deng, V. Gersuk, A. K. Shalek, C. K. Slichter, H. W. Miller, M. J. McElrath, M. Prlic, et al. MAST: a flexible statistical framework for assessing transcriptional changes and characterizing heterogeneity in single-cell RNA sequencing data. *Genome biology*, 16(1):1–13, 2015.

[12] C. Hafemeister and R. Satija. Normalization and variance stabilization of single-cell RNA-seq data using regularized negative binomial regression. *Genome biology*, 20(1):1–15, 2019.

[13] H. M. Kang, M. Subramaniam, S. Targ, M. Nguyen, L. Maliskova, E. McCarthy, E. Wan, S. Wong, L. Byrnes, C. M. Lanata, et al. Multiplexed droplet single-cell RNA-sequencing using natural genetic variation. *Nature biotechnology*, 36(1):89, 2018.

[14] P. V. Kharchenko, L. Silberstein, and D. T. Scadden. Bayesian approach to single-cell differential expression analysis. *Nature methods*, 11(7):740–742, 2014.

[15] K. D. Korthauer, L.-F. Chu, M. A. Newton, Y. Li, J. Thomson, R. Stewart, and C. Kendziorski. A statistical approach for identifying differential distributions in single-cell RNA-seq experiments. *Genome biology*, 17(1):222, 2016.

[16] M. I. Love, W. Huber, and S. Anders. Moderated estimation of fold change and dispersion for RNA-seq data with DESeq2. *Genome biology*, 15(12):550, 2014.

[17] A. Lütge, J. Zyprych-Walczak, U. B. Kunzmann, H. L. Crowell, D. Calini, D. Malhotra, C. Soneson, and M. D. Robinson. Cellmixs: quantifying and visualizing batch effects in single-cell rna-seq data. *Life science alliance*, 4(6), 2021.

[18] F. J. Massey Jr. The kolmogorov-smirnov test for goodness of fit. *Journal of the American statistical Association*, 46(253):68–78, 1951.

[19] D. J. McCarthy, K. R. Campbell, A. T. Lun, and Q. F. Wills. Scater: pre-processing, quality control, normalization and visualization of single-cell RNA-seq data in R. *Bioinformatics*, 33(8):1179–1186, 2017.

[20] M. Nowicka, C. Krieg, L. M. Weber, F. J. Hartmann, S. Guglietta, B. Becher, M. P. Levesque, and M. D. Robinson. CyTOF workflow: differential discovery in high-throughput high-dimensional cytometry datasets. *F1000Research*, 6, 2017.

[21] B. Phipson and G. K. Smyth. Permutation p-values should never be zero: Calculating exact p-values when permutations are randomly drawn. *Statistical applications in genetics and molecular biology*, 9:Article39, 2010.

[22] X.-Q. Qin, N. Tao, A. Dergay, P. Moy, S. Fawell, A. Davis, J. M. Wilson, and J. Barsoum. Interferon-$\beta$ gene therapy inhibits tumor formation and causes regression of established tumors in immune-deficient mice. *Proceedings of the National Academy of Sciences*, 95(24):14411–14416, 1998.

[23] M. E. Ritchie, B. Phipson, D. Wu, Y. Hu, C. W. Law, W. Shi, and G. K. Smyth. limma powers differential expression analyses for RNA-sequencing and microarray studies. *Nucleic acids research*, 43(7):e47–e47, 2015.

842 [24] M. D. Robinson, D. J. McCarthy, and G. K. Smyth. edgeR: a Bioconductor
843 package for differential expression analysis of digital gene expression data.
844 *Bioinformatics*, 26(1):139–140, 2010.

845 [25] C. Soneson and M. D. Robinson. Bias, robustness and scalability in single-
846 cell differential expression analysis. *Nature methods*, 15(4):255, 2018.

847 [26] J. W. Squair, M. Gautier, C. Kathe, M. A. Anderson, N. D. James, T. H.
848 Hutson, R. Hudelle, T. Qaiser, K. J. Matson, Q. Barraud, et al. Confronting
849 false discoveries in single-cell differential expression. *bioRxiv*, 2021.

850 [27] P.-Y. Tung, J. D. Blischak, C. J. Hsiao, D. A. Knowles, J. E. Burnett, J. K.
851 Pritchard, and Y. Gilad. Batch effects and the effective design of single-cell
852 gene expression studies. *Scientific reports*, 7:39921, 2017.

853 [28] M. Uhlén, L. Fagerberg, B. M. Hallström, C. Lindskog, P. Oksvold,
854 A. Mardinoglu, Å. Sivertsson, C. Kampf, E. Sjöstedt, A. Asplund, et al.
855 Tissue-based map of the human proteome. *Science*, 347(6220), 2015.

856 [29] C. A. Vallejos, J. C. Marioni, and S. Richardson. BASiCS: Bayesian
857 analysis of single-cell sequencing data. *PLoS computational biology*,
858 11(6):e1004333, 2015.

859 [30] C. A. Vallejos, S. Richardson, and J. C. Marioni. Beyond comparisons of
860 means: understanding changes in gene expression at the single-cell level.
861 *Genome biology*, 17(1):1–14, 2016.

862 [31] T. Wang, B. Li, C. E. Nelson, and S. Nabavi. Comparative analysis of dif-
863 ferential gene expression analysis tools for single-cell RNA sequencing data.
864 *BMC bioinformatics*, 20(1):40, 2019.

865 [32] L. M. Weber, M. Nowicka, C. Soneson, and M. D. Robinson. diffcyt: Differ-
866 ential discovery in high-dimensional cytometry via high-resolution cluster-
867 ing. *Communications biology*, 2(1):1–11, 2019.

868 [33] L. M. Weber and C. Soneson. Hdcytodata: Collection of high-
869 dimensional cytometry benchmark datasets in bioconductor object formats.
870 *F1000Research*, 8, 2019.

871 [34] S. H. Yip, P. Wang, J.-P. A. Kocher, P. C. Sham, and J. Wang. Linnorm: im-
872 proved statistical analysis for single cell RNA-seq expression data. *Nucleic
873 acids research*, 45(22):e179–e179, 2017.

874 [35] L. Zappia, B. Phipson, and A. Oshlack. Splatter: simulation of single-cell
875 RNA sequencing data. *Genome biology*, 18(1):1–15, 2017.

876 [36] Y. Zhang, L. Zheng, L. Zhang, X. Hu, X. Ren, and Z. Zhang. Deep single-cell
877 RNA sequencing data of individual T cells from treatment-naive colorectal
878 cancer patients. *Scientific data*, 6(1):1–15, 2019.